Monthly Notices of the ROYAL ASTRONOMICAL SOCIETY

MNRAS **460,** 3861–3872 (2016)
Advance Access publication 2016 May 23

doi:10.1093/mnras/stw1237

# Herschel protocluster survey: a search for dusty star-forming galaxies in protoclusters at $z = 2$–3

Y. Kato,[1,2★] Y. Matsuda,[1,3] Ian Smail,[4,5] A. M. Swinbank,[4,5] B. Hatsukade,[1] H. Umehata,[6,7] I. Tanaka,[8] T. Saito,[1] D. Iono,[1,3] Y. Tamura,[7] K. Kohno,[7,9] D. K. Erb,[10] B. D. Lehmer,[11] J. E. Geach,[12] C. C. Steidel,[13] D. M. Alexander,[4] T. Yamada[14] and T. Hayashino[15]

[1]*National Astronomical Observatory of Japan, 2-21-1 Osawa, Mitaka, Tokyo 181-8588, Japan*
[2]*Department of Astronomy, Graduate school of Science, The University of Tokyo, 7-3-1 Hongo, Bunkyo-ku, Tokyo 133-0033, Japan*
[3]*Department of Astronomy, School of Science, The Graduate University for Advanced Studies (SOKENDAI), Osawa, Mitaka, Tokyo 181-8588, Japan*
[4]*Centre for Extragalactic Astronomy, Department of Physics, Durham University, South Road, Durham DH1 3LE, UK*
[5]*Institute for Computational Cosmology, Durham University, South Road, Durham DH1 3LE, UK*
[6]*European Southern Observatory, Karl-Schwarzschild-Str. 2, D-85748 Garching, Germany*
[7]*Institute of Astronomy, School of Science, The University of Tokyo, 2-21-1 Osawa, Mitaka, Tokyo 181-0015, Japan*
[8]*Subaru Telescope, National Astronomical Observatory of Japan, 650 North Aohoku Place, Hilo, HI 96720, USA*
[9]*Research Center for the Early Universe, The University of Tokyo, 7-3-1 Hongo, Bunkyo, Tokyo 113-0033, Japan*
[10]*Center for Gravitation, Cosmology and Astrophysics, Department of Physics, University of Wisconsin Milwaukee, 3135 North Maryland Avenue, Milwaukee, WI 53211, USA*
[11]*Department of Physics, University of Arkansas, 226 Physics Building, 835 West Dickson Street, Fayetteville, AR 72701, USA*
[12]*Centre for Astrophysics Research, Science and Technology Research Institute, University of Hertfordshire, Hatfield AL10 9AB, UK*
[13]*California Institute of Technology, MS 249-17, Pasadena, CA 91125, USA*
[14]*Institute of Space Astronautical Science, Japan Aerospace Exploration Agency, Sagamihara, Kanagawa 252-5210, Japan*
[15]*Research Center for Neutrino Science, Tohoku University, Sendai, Miyagi 980-8578, Japan*

Accepted 2016 May 19. Received 2016 May 16; in original form 2016 March 18

## ABSTRACT

We present a *Herschel*/Spectral and Photometric Imaging Receiver (SPIRE) survey of three protoclusters at $z = 2$–3 (2QZCluster, HS1700, SSA22). Based on the SPIRE colours ($S_{350}/S_{250}$ and $S_{500}/S_{350}$) of 250 μm sources, we selected high-redshift dusty star-forming galaxies potentially associated with the protoclusters. In the 2QZCluster field, we found a 4$\sigma$ overdensity of six SPIRE sources around 4.5 arcmin (∼2.2 Mpc) from a density peak of H $\alpha$ emitters at $z = 2.2$. In the HS1700 field, we found a 5$\sigma$ overdensity of eight SPIRE sources around 2.1 arcmin (∼1.0 Mpc) from a density peak of Lyman-break galaxies at $z = 2.3$. We did not find any significant overdensities in SSA22 field, but we found three 500 μm sources are concentrated 3 arcmin (∼1.4 Mpc) east to the Ly $\alpha$ emitters overdensity. If all the SPIRE sources in these three overdensities are associated with protoclusters, the inferred star formation rate densities are $10^3$–$10^4$ times higher than the average value at the same redshifts. This suggests that dusty star formation activity could be very strongly enhanced in $z \sim 2$–3 protoclusters. Further observations are needed to confirm the redshifts of the SPIRE sources and to investigate what processes enhance the dusty star formation activity in $z \sim 2$–3 protoclusters.

**Key words:** galaxies: formation – galaxies: high-redshift – infrared: galaxies – submillimetre: galaxies.

## 1 INTRODUCTION

The central regions of local clusters are dominated by passive early-type ellipticals and spheroidals, their stellar populations are old, with inferred formation redshifts of $z \gtrsim 2$ (e.g. Ellis et al. 1997). High-redshift dusty star-forming galaxies (DSFGs) are strongly star-forming galaxies [star formation rate (SFR) $\gtrsim$100–1000 $M_\odot$ $yr^{-1}$] and have been proposed to the precursors of present-day ellipticals in local clusters (e.g. Lilly et al. 1998; Smail et al. 1998; Lutz et al. 2001; Ivison et al. 2013). Large hydrodynamical simulations and galaxy formation models predict intense star formation could be

★E-mail: kato.yu@nao.ac.jp

**Table 1.** Summary of our *Herschel*/SPIRE observations.

| Target | $z^a$ | RA$^b$ (J2000) | Dec.$^c$ (J2000) | Area$^d$ (arcmin$^2$) | $t_{\rm int}{}^e$ (h) | $\sigma_{\rm conf}{}^f$ $S_{250}$ (mJy) | $S_{350}$ (mJy) | $S_{500}$ (mJy) | $\sigma_{\rm inst}{}^g$ $S_{250}$ (mJy) | $S_{350}$ (mJy) | $S_{500}$ (mJy) |
|---|---|---|---|---|---|---|---|---|---|---|---|
| 2QZCluster | $2.230 \pm 0.016$ | $10^{\rm h}03^{\rm m}51^{\rm s}$ | $+00^{\rm d}15^{\rm m}09^{\rm s}$ | 515 | 1.8 | 6.7 | 7.0 | 7.1 | 2.0–3.9 | 1.6–2.6 | 2.0–3.3 |
| HS1700 | $2.300 \pm 0.015$ | $17^{\rm h}01^{\rm m}15^{\rm s}$ | $+64^{\rm d}14^{\rm m}03^{\rm s}$ | 497 | 1.5 | 7.3 | 7.4 | 7.5 | 2.0–3.7 | 1.6–2.7 | 2.0–3.2 |
| SSA22 | $3.09 \pm 0.03$ | $22^{\rm h}17^{\rm m}34^{\rm s}$ | $+00^{\rm d}17^{\rm m}01^{\rm s}$ | 1076 | 3.7 | 7.7 | 7.8 | 8.0 | 1.9–3.2 | 1.6–2.4 | 1.9–3.0 |
| COSMOS | – | $10^{\rm h}00^{\rm m}37^{\rm s}$ | $+02^{\rm d}11^{\rm m}26^{\rm s}$ | 3422 | 50.1 | 7.1 | 7.7 | 7.8 | 2.1–2.7 | 1.7–2.0 | 2.1–2.8 |

[a]Redshift range of the member galaxies, based on HAEs for 2QZCluster (Matsuda et al. 2011) and LBGs for HS1700 (Steidel et al. 2005) and SSA22 (Steidel et al. 1998, 2000).
[b,c]The coordinates of the field centre of *Herschel*/SPIRE observations.
[d]The area where the integration time is greater than 30 per cent. For COSMOS field, we used centre of 3422 arcmin$^2$ area. We detected sources within this area (see also Fig. 3).
[e]The total integration time. For the survey design of COSMOS field, please see Oliver et al. (2012).
[f,g]The confusion noise and instrumental noise.

detectable as concentrations of DSFGs in $z \gtrsim 2$ protoclusters (e.g. Granato et al. 2015). Indeed, there have been reports of a reversal of the SFR-density relation (e.g. Elbaz et al. 2007; Tran et al. 2010), which is increasing SFR with increasing local density at $z \gtrsim 1$. Protoclusters at $z \gtrsim 2$ are thus unique laboratories to explore bursting star-formation in a critical epoch of galaxy formation (Casey 2016).

A number of studies have confirmed the presence of DSFGs in $z < 2$ galaxy clusters (e.g. Brodwin et al. 2013; Smail et al. 2014; Ma et al. 2015; Webb et al. 2015), while studies confirming DSFGs at $z \gtrsim 2$ protoclusters are also progressing (e.g. Tamura et al. 2009; Clements et al. 2014; Umehata et al. 2014, 2015; Casey et al. 2015). Some surveys to search for DSFGs at far-infrared (FIR) wavelengths have focused on radio galaxy fields (e.g. Stevens et al. 2003; Valtchanov et al. 2013; Dannerbauer et al. 2014; Rigby et al. 2014). Radio galaxies are thought to be tracers of large-scale structures, and some fraction of $z \gtrsim 2$ protoclusters around radio galaxies indeed appear to have experienced bursting dusty star formation related to DSFGs (e.g. Ivison et al. 2000). However, such regions may be biased by the end to host a currently accreting supermassive black hole and so we also need to explore DSFGs large-scale structures selected by other techniques at $z \gtrsim 2$ to investigate bursting star formation more generally. Clements et al. (2014) investigated ~90 deg$^2$ sky observed as part of the *Herschel* Multi-tiered Extragalactic survey (HerMES) with *Planck* and *Herschel* to search for clusters undergoing dusty star formation. They found four candidate clusters, and for all four cases they found evidence of galaxy clusters with red sequence based on optical/NIR data. The SFR density of these at $z \gtrsim 2$ are four order of magnitudes higher than the cosmic averaged values. But is this also true for dusty star formation in known optical/UV-selected galaxy clusters at $z \gtrsim 2$?

In this paper, we report a result of observations with the Spectral and Photometric Imaging Receiver (SPIRE; Griffin et al. 2010) on the *Herschel Space Observatory* (Pilbratt et al. 2010) for three protoclusters at $z = 2$–3 (2QZCluster, HS1700, and SSA22 at $z = 2.2$, 2.3, and 3.1, respectively). The three protoclusters have filamentary, large-scale structures of rest-frame UV to optical selected galaxies. The structure of this paper is as follows. In Section 2, we introduce the *Herschel*/SPIRE observations, the data processing, and our targeted fields. In Section 3, we present source detection methods, number counts, and SPIRE colour selection. In Sections 4 and 5, we present our results, discussion, and then summarize our main findings. We use the following cosmological parameters: $\Omega_{\rm m} = 0.3$, $\Omega_\Lambda = 0.7$, $h = 0.7$. In this cosmology, the Universe is 2.9, 2.8, and 2.0 Gyr old and 1.0 arcsec corresponds to 8.3, 8.2, and 7.6 kpc in physical length at $z = 2.2$, 2.3, and 3.1, respectively.

## 2 OBSERVATIONS AND TARGET FIELDS

### 2.1 SPIRE observations

Our *Herschel*/SPIRE observations were performed as part of the second Open Time *Herschel* programmes (PI: Y. Matsuda). We summarize the observations in Table 1. The observations were executed in Large Map mode with a scan rate of 30 arcsec s$^{-1}$, repeated 14 times for each field ($N_{\rm rep} = 14$). The dates of observations are 2012 June 22 (2QZCluster), 2012 March 4 (HS1700), and 2012 May 10 (SSA22). The coverage of the maps are ~23 arcmin × 23 arcmin (2QZCluster), ~22 arcmin × 22 arcmin (HS1700), and ~33 arcmin × 33 arcmin (SSA22) corresponding to ~40–60 comoving Mpc at the protocluster redshifts, which are sufficient to search for concentration of DSFGs around the density peak of protocluster members. The integration times are 1.8, 1.5, and 3.7 h for 2QZCluster, HS1700, and SSA22, respectively. Maps were produced with the *Herschel* Interactive Processing Environment (HIPE, v11.0.0), following the standard data processing and map-making steps with destriping. The full width at half-maximum (FWHM) of the SPIRE beam is 18.1, 24.9, and 36.6 arcsec at 250, 350, and 500 μm, respectively (Swinyard et al. 2010). The final maps have pixel sizes of 6, 10, and 14 arcsec at 250, 350, and 500 μm. We measured the 1$\sigma$ confusion noise ($\sigma_{\rm conf}$) as map variance of flux density within effective area (Table 1), which are slightly higher than the values of blank fields (Nguyen et al. 2010). The instrumental noise measured in our three protoclusters is about one-third of the confusion noise (Table 1).

### 2.2 Protocluster targets

2QZCluster: this protocluster was originally identified as a concentration of five quasi-stellar objects (QSOs) in a ~1 deg region at $z = 2.23$ from the 2dF Quasar Redshift survey (Croom et al. 2001, 2004). Four out of the five QSOs are even more strongly clustered in a 30 × 30 comoving Mpc patch. An H$\alpha$ narrow-band imaging revealed a filamentary large-scale structure of an overdensity of 22 H$\alpha$ emittes (HAEs) connecting the QSOs (Matsuda et al. 2011). *Chandra*/Advanced CCD Imaging Spectrometer (ACIS) 100 ks observations of this structure also showed evidence that the active galactic nucleus (AGN) fraction is a factor of ~3.5 higher than blank fields (Lehmer et al. 2013).

**Table 2.** Summary of *Herschel*/SPIRE sources in the three protoclusters.

| Field | Area[a] (arcmin$^{-2}$) | $N^b$ (prior) | $N^c$ (catalogued) | $N^d$ (selected) | $N^e$ | $\Sigma^f$ (arcmin$^{-2}$) | $\Sigma^g$ (arcmin$^{-2}$) | $\delta^h$ | $\sigma^i$ |
|---|---|---|---|---|---|---|---|---|---|
| 2QZCluster | 515 | 643 | 399 | 12 | 6 | $0.023 \pm 0.007$ | $0.132 \pm 0.054$ | $3.0 \pm 1.7$ | $3.9 \pm 2.1$ |
| HS1700 | 497 | 579 | 383 | 26 | 8 | $0.052 \pm 0.010$ | $0.186 \pm 0.066$ | $3.7 \pm 1.7$ | $5.0 \pm 2.2$ |
| SSA22 | 1076 | 1253 | 772 | 55 | 5 | $0.051 \pm 0.007$ | – | – | – |
| COSMOS (matched to 2QZCluster) | 3422 | 4923 | 2777 | 111 | 7 | $0.032 \pm 0.003$ | – | – | – |
| COSMOS (matched to HS1700) | 3422 | 4923 | 2777 | 140 | 7 | $0.041 \pm 0.004$ | – | – | – |
| COSMOS (matched to SSA22) | 3422 | 4923 | 2777 | 262 | 10 | $0.077 \pm 0.005$ | – | – | – |

[a]The area where the integration time is greater than 30 per cent. We detected sources within this area.
[b]The numbers of S/N (250 μm) > 2 prior sources.
[c]The numbers of catalogued sources which at least one SPIRE band flux is above 12 mJy.
[d]The numbers of colour-selected bright SPIRE sources. For SSA22, we excluded the sources in high background fluxes (see Fig. 3).
[e]The numbers of colour-selected bright SPIRE sources within the overdensities.
[f]The surface density of colour-selected bright SPIRE sources. The errors assume Poisson statistics.
[g]The surface density of colour-selected bright SPIRE sources in the overdensities, assume an area of the overdensities ($r = 3.8$ arcmin for 2QZCluster, $r = 3.7$ arcmin for HS1700). The errors assume Poisson statistics.
[h,i]The $\delta$ and $\sigma$ are calculated from $\delta_{\rm pc} = (n_{\rm pc} - n_{\rm ave})/n_{\rm ave}$ and $\sigma_{\rm pc} = (n_{\rm pc} - n_{\rm ave})/\sigma_{\rm ave}$. The errors assume Poisson statistics.

**Table 3.** SPIRE sources catalogue of 2QZCluster. The full table is available online.

| ID | RA (J2000) | Dec. (J2000) | $S_{250}$ (mJy) | $S_{350}$ (mJy) | $S_{500}$ (mJy) |
|---|---|---|---|---|---|
| 2QZCluster-SPIRE1 | 150.818 469 683 681 12 | 0.029 424 092 103 377 656 | $127.0 \pm 2.1$ | $54.2 \pm 1.9$ | $24.6 \pm 2.2$ |
| 2QZCluster-SPIRE2 | 150.764 809 504 820 65 | 0.225 012 546 982 003 38 | $139.1 \pm 2.4$ | $117.9 \pm 1.8$ | $71.4 \pm 2.3$ |
| 2QZCluster-SPIRE3 | 150.915 179 596 640 77 | 0.390 983 346 292 9028 | $111.4 \pm 2.4$ | $55.2 \pm 1.8$ | $21.2 \pm 2.4$ |
| 2QZCluster-SPIRE4 | 151.024 635 066 809 82 | 0.120 654 182 340 4277 | $97.4 \pm 2.2$ | $54.2 \pm 1.8$ | $26.5 \pm 2.4$ |
| 2QZCluster-SPIRE5 | 151.044 557 622 064 53 | 0.404 733 993 735 9634 | $93.6 \pm 2.3$ | $61.3 \pm 1.8$ | $24.2 \pm 2.2$ |
| 2QZCluster-SPIRE6 | 151.079 307 187 455 27 | 0.120 069 119 139 769 63 | $84.1 \pm 2.3$ | $58.9 \pm 1.8$ | $31.3 \pm 2.3$ |
| 2QZCluster-SPIRE7 | 151.112 251 221 980 36 | 0.176 742 195 939 817 88 | $66.1 \pm 2.2$ | $36.2 \pm 2.1$ | $13.2 \pm 2.1$ |
| 2QZCluster-SPIRE8 | 150.706 609 115 4151 | 0.283 058 550 203 0584 | $67.4 \pm 2.3$ | $54.5 \pm 1.8$ | $18.4 \pm 2.2$ |
| 2QZCluster-SPIRE9 | 150.949 687 759 857 14 | 0.331 169 788 149 76 | $64.4 \pm 2.2$ | $22.2 \pm 1.9$ | $0.0 \pm 2.1$ |
| 2QZCluster-SPIRE10 | 150.916 319 779 268 35 | 0.352 455 847 951 7708 | $60.1 \pm 2.1$ | $64.7 \pm 1.8$ | $45.6 \pm 2.0$ |

HS1700: this protocluster was originally discovered as a ∼7 × density contrast redshift spike of UV/optical-selected star-forming galaxies (BX/BM) within a ∼25 comoving Mpc region at $z = 2.30$ (Steidel et al. 2005). A Ly $\alpha$ narrow-band imaging survey revealed a filamentary large-scale structure of six giant Ly $\alpha$ Blobs(LABs; Erb, Bogosavljević & Steidel 2011). *Chandra*/ACIS-I 200 ks observations of this structure also showed tentative evidence of an enhancement of AGN fraction compared to the field environment (Digby-North et al. 2010).

SSA22: this protocluster was originally discovered as a ∼4–6 × density contrast in redshift distribution of Lyman-break galaxies (LBGs) and Ly $\alpha$ emitters (LAEs) within a ∼20 comoving Mpc region at $z = 3.09$ (Steidel et al. 1998, 2000). A wide-field Ly $\alpha$ narrow-band imaging survey with Subaru Telescope revealed a filamentary large-scale structure of 283 LAEs, extended to at least ∼60 comoving Mpc (Hayashino et al. 2004). This sample of LAEs includes 35 LABs with sizes of 30–150 kpc scale (Steidel et al. 2000; Matsuda et al. 2004). *Chandra*/ACIS-I 400 ks observations of this structure showed that the AGN fraction of protocluster members is ∼3 × higher than that in the field environment (Lehmer et al. 2009a,b).

Blank field (COSMOS): we have chosen well-studied extragalactic field Cosmic Evolution Survey (COSMOS) to use as a blank field, which is observed as a part of HerMES (Oliver et al. 2012). The SPIRE map in COSMOS field is larger and deeper than our observations, so we have reprocessed them by limiting to the same depth using $N_{\rm rep} = 14$. Subsequently, we apply the same map making, and source detection procedure in order to make sure that we match the depth of our observations. The confusion and instrumental noise values are given in Table 1.

## 3 ANALYSIS

### 3.1 DETECTION AND NUMBER COUNTS

The source detection was conducted on the 250 μm maps, because of the better spatial resolution compared with longer wavelength bands. We caution that 500 μm detection causes a source blending (even 250 μm can deblend these) and large spatial uncertainty. We used the SUSSEXTRACTOR (Smith et al. 2012) for the source detection and photometry. We detected S/N > 2 sources in the maps within the region where the integration time is greater than 30 per cent of the deepest parts (515 arcmin$^2$ for 2QZCluster, 497 arcmin$^2$ for HS1700, 1076 arcmin$^2$ for SSA22, and 3422 arcmin$^2$ for COSMOS field). We measured 350 and 500 μm fluxes at the positions of sources detected in the 250 μm maps, then listed these 250 μm sources only if the flux density is above 12 mJy in at least one of the SPIRE bands (See also Table 3–5, and the full tables are available online). This flux density limit corresponds to ∼4$\sigma$ of the instrumental noise and ∼2$\sigma$ of the confusion noise in all three bands. For SSA22, we cut out the region shown in Fig. 3 due to the high background fluxes from the Galactic cirrus.

We compared these SPIRE number counts with COSMOS field. We show the raw (i.e. not corrected for the completeness) number counts in Fig. 1 (See also Table 6–9). The raw number counts are roughly consistent with COSMOS field data at >20 mJy bin at 250

**Table 4.** SPIRE sources catalogue of HS1700. The full table is available online.

| ID | RA (J2000) | Dec. (J2000) | $S_{250}$ (mJy) | $S_{350}$ (mJy) | $S_{500}$ (mJy) |
|---|---|---|---|---|---|
| HS1700-SPIRE1 | 255.536 466 830 569 28 | 64.206 008 325 3161 | 422.6 ± 3.1 | 181.4 ± 1.9 | 67.3 ± 2.4 |
| HS1700-SPIRE2 | 255.070 942 026 801 16 | 64.363 372 461 877 29 | 112.4 ± 2.2 | 49.0 ± 1.9 | 19.5 ± 2.2 |
| HS1700-SPIRE3 | 255.105 114 624 299 38 | 64.146 862 046 926 69 | 86.2 ± 2.4 | 51.5 ± 2.0 | 21.4 ± 2.1 |
| HS1700-SPIRE4 | 255.158 064 741 439 26 | 64.229 161 354 827 77 | 85.8 ± 2.5 | 60.5 ± 1.8 | 27.9 ± 2.2 |
| HS1700-SPIRE5 | 254.994 378 530 705 03 | 64.264 103 806 346 14 | 70.8 ± 2.1 | 76.4 ± 1.7 | 51.2 ± 2.2 |
| HS1700-SPIRE6 | 254.918 630 411 580 92 | 64.211 743 084 186 98 | 76.7 ± 2.4 | 44.4 ± 1.7 | 17.6 ± 2.3 |
| HS1700-SPIRE7 | 255.223 598 432 973 63 | 64.386 465 219 551 37 | 65.7 ± 2.2 | 21.3 ± 1.9 | 13.0 ± 2.3 |
| HS1700-SPIRE8 | 254.829 380 212 913 24 | 64.178 731 079 895 98 | 68.7 ± 2.3 | 59.4 ± 1.7 | 27.6 ± 2.2 |
| HS1700-SPIRE9 | 255.201 687 559 440 53 | 64.258 590 551 266 69 | 66.3 ± 2.2 | 35.3 ± 2.1 | 16.2 ± 2.2 |
| HS1700-SPIRE10 | 255.182 354 384 1818 | 64.031 533 725 227 55 | 64.7 ± 2.2 | 64.8 ± 1.9 | 31.2 ± 2.1 |

**Table 5.** SPIRE sources catalogue of SSA22. The full table is available online.

| ID | RA (J2000) | Dec. (J2000) | $S_{250}$ (mJy) | $S_{350}$ (mJy) | $S_{500}$ (mJy) |
|---|---|---|---|---|---|
| SSA22-SPIRE1 | 334.264 444 128 561 | 0.676 441 558 620 3842 | 135.3 ± 2.2 | 71.3 ± 1.9 | 30.4 ± 2.3 |
| SSA22-SPIRE2 | 334.571 606 842 402 56 | 0.492 191 614 225 445 83 | 93.3 ± 2.2 | 76.7 ± 1.7 | 48.7 ± 2.3 |
| SSA22-SPIRE3 | 334.344 178 441 303 | 0.352 865 223 284 7903 | 79.2 ± 2.2 | 34.4 ± 1.9 | 10.4 ± 2.2 |
| SSA22-SPIRE4 | 334.344 575 729 272 44 | 0.607 307 593 915 126 | 79.7 ± 2.4 | 56.9 ± 1.7 | 21.9 ± 2.0 |
| SSA22-SPIRE5 | 334.697 451 156 846 17 | 0.398 383 690 170 6686 | 72.9 ± 2.2 | 29.8 ± 1.9 | 12.8 ± 2.1 |
| SSA22-SPIRE6 | 334.392 819 716 858 | 0.304 233 265 249 4624 | 68.9 ± 2.1 | 33.2 ± 1.8 | 0.0 ± 2.1 |
| SSA22-SPIRE7 | 334.238 362 745 988 24 | 0.401 941 586 060 649 45 | 61.8 ± 2.1 | 45.8 ± 1.8 | 8.8 ± 2.1 |
| SSA22-SPIRE8 | 334.554 628 306 314 44 | 0.477 018 638 267 817 65 | 62.9 ± 2.1 | 33.3 ± 1.8 | 18.3 ± 2.0 |
| SSA22-SPIRE9 | 334.384 899 903 3597 | 0.291 239 586 624 6295 | 57.5 ± 2.1 | 49.6 ± 1.7 | 45.7 ± 2.2 |
| SSA22-SPIRE10 | 334.580 022 165 982 03 | 0.350 067 987 634 731 85 | 64.3 ± 2.3 | 51.3 ± 2.0 | 30.6 ± 2.3 |

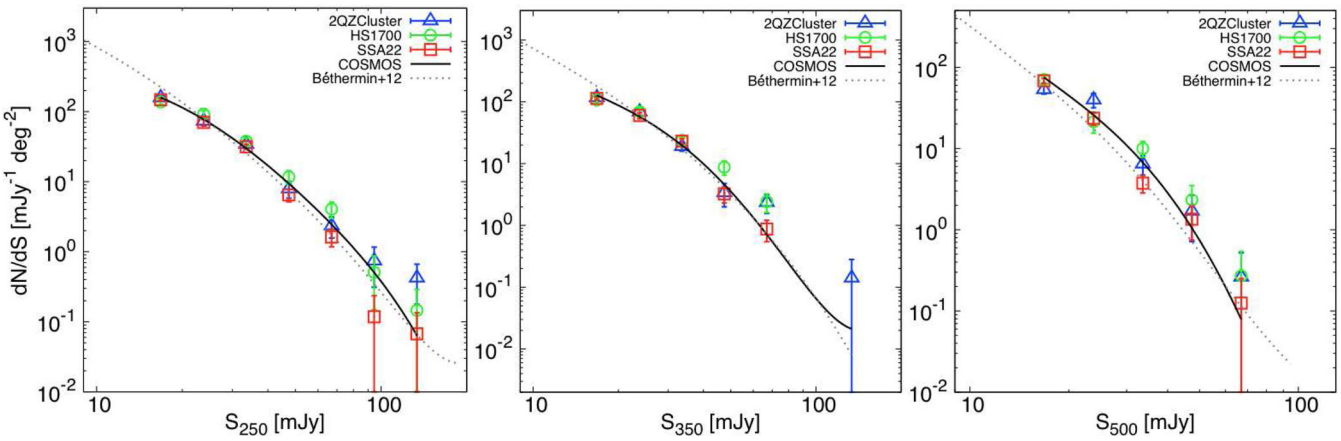


**Figure 1.** Number counts at 250, 350, and 500 μm in the three protoclusters and COSMOS field. We detected S/N > 2 sources in the 250 μm maps and measured the 350 and 500 μm fluxes at the positions of the 250 μm sources. We fitted the data points of COSMOS field with a bézier curve. The number counts of the SPIRE sources in the protoclusters averaged over their full fields are roughly consistent with those of COSMOS field. The number counts of the SPIRE sources in COSMOS field are also consistent with those of HerMES blank fields (Béthermin et al. 2012), suggesting that COSMOS field can be used as a control field.

**Table 6.** Number of sources which have fluxes above 12 mJy in each bands.

| | COSMOS | SSA22 | HS1700 | 2QZCluster |
|---|---|---|---|---|
| 250 μm | 2552 | 699 | 356 | 365 |
| 350 μm | 1944 | 529 | 259 | 260 |
| 500 μm | 961 | 252 | 133 | 116 |

and 350 μm. A moderate excess of number counts at $S_{350} > 50$ mJy and $S_{500} > 40$ mJy were found (by a factor of 2–3) in HS1700 and 2QZCluster, although they are within the error bars based on Poisson noise. We also compared number counts in COSMOS field with wider HerMES survey data (Béthermin et al. 2012). The number counts in COSMOS field agree with that of HerMES survey data, suggesting that COSMOS field is suitable as a control field.

**Table 7.** Number counts at 250 μm. The errors take into account the statistical uncertainties, including the Poisson noise.

| Central flux (mJy) | Flux bin (mJy) | Number counts (d$N$/d$S$) [mJy$^{-1}$ deg$^{-2}$] SSA22 | HS1700 | 2QZCluster | COSMOS |
|---|---|---|---|---|---|
| 16.8 | 12.0–21.6 | 148.1 ± 7.2 | 137.2 ± 10.2 | 157.1 ± 10.7 | 158.1 ± 4.2 |
| 23.8 | 21.6–26.0 | 70.0 ± 7.3 | 92.1 ± 12.3 | 73.0 ± 10.8 | 87.5 ± 4.6 |
| 33.6 | 26.0–41.2 | 31.5 ± 2.6 | 37.6 ± 4.2 | 34.0 ± 4.0 | 36.4 ± 1.6 |
| 47.4 | 41.2–53.6 | 6.5 ± 1.3 | 11.7 ± 2.6 | 7.9 ± 2.1 | 10.4 ± 0.9 |
| 67.0 | 53.6–80.4 | 1.6 ± 0.5 | 4.0 ± 1.0 | 2.3 ± 0.8 | 2.7 ± 0.3 |
| 94.6 | 80.4–108.8 | 0.12 ± 0.12 | 0.51 ± 0.36 | 0.74 ± 0.43 | 0.74 ± 0.17 |
| 133.7 | 108.8–158.6 | 0.07 ± 0.07 | 0.15 ± 0.15 | 0.42 ± 0.24 | 0.06 ± 0.04 |
| 188.8 | 158.6–219.0 | – | – | – | – |

**Table 8.** Number counts at 350 μm. The errors take into account the statistical uncertainties, including the Poisson noise.

| Central flux (mJy) | Flux bin (mJy) | Number counts (d$N$/d$S$) [mJy$^{-1}$ deg$^{-2}$] SSA22 | HS1700 | 2QZCluster | COSMOS |
|---|---|---|---|---|---|
| 16.8 | 12.0–21.6 | 113.6 ± 6.3 | 107.0 ± 9.0 | 116.4 ± 9.2 | 127.4 ± 3.7 |
| 23.8 | 21.6–26.0 | 60.1 ± 6.8 | 69.1 ± 10.7 | 68.3 ± 10.4 | 62.2 ± 3.9 |
| 33.6 | 26.0–41.2 | 23.1 ± 2.3 | 23.8 ± 3.4 | 18.8 ± 2.9 | 28.5 ± 1.4 |
| 47.4 | 41.2–53.6 | 3.2 ± 0.9 | 8.8 ± 2.3 | 3.4 ± 1.4 | 5.9 ± 0.7 |
| 67.0 | 53.6–80.4 | 0.9 ± 0.3 | 2.4 ± 0.8 | 2.3 ± 0.8 | 1.5 ± 0.2 |
| 94.6 | 80.4–108.8 | – | – | – | 0.04 ± 0.04 |
| 133.7 | 108.8–158.6 | – | – | 0.14 ± 0.14 | – |
| 188.8 | 158.6–219.0 | – | – | – | – |

**Table 9.** Number counts at 500 μm. The errors take into account the statistical uncertainties, including the Poisson noise.

| Central flux (mJy) | Flux bin (mJy) | Number counts (d$N$/d$S$) [mJy$^{-1}$ deg$^{-2}$] SSA22 | HS1700 | 2QZCluster | COSMOS |
|---|---|---|---|---|---|
| 16.8 | 12.0–21.6 | 68.3 ± 4.9 | 70.8 ± 7.3 | 53.1 ± 6.2 | 75.2 ± 2.9 |
| 23.8 | 21.6–26.0 | 23.6 ± 4.2 | 21.4 ± 5.9 | 39.7 ± 7.9 | 27.3 ± 2.6 |
| 33.6 | 26.0–41.2 | 3.7 ± 0.9 | 10.0 ± 2.2 | 6.4 ± 1.7 | 9.7 ± 0.8 |
| 47.4 | 41.2–53.6 | 1.3 ± 0.6 | 2.3 ± 1.2 | 1.7 ± 1.0 | 1.6 ± 0.4 |
| 67.0 | 53.6–80.4 | 0.1 ± 0.1 | 0.27 ± 0.27 | 0.26 ± 0.26 | 0.08 ± 0.06 |
| 94.6 | 80.4–108.8 | – | – | – | – |
| 133.7 | 108.8–158.6 | – | – | – | – |
| 188.8 | 158.6–219.0 | – | – | – | – |

### 3.2 SPIRE colour selection

In order to search for DSFGs possibly associated with the protoclusters, we applied a colour constraint to the SPIRE-detected sources. The $S_{350}/S_{250}$ and $S_{500}/S_{350}$ colours were used to select the sources with single grey-body spectral energy distributions (SEDs) at the protocluster's redshift ranges, with dust temperatures of $T_d = 30$–40 K, and a dust emissivity $\beta = 1.5$. Casey et al. (2012) measured the dust temperatures of SPIRE-selected DSFGs and showed that they are in the range of $T_d = 20$–60 K. The dust-emissivity index is determined by Hildebrand (1983), and typically $\beta = 1.0$–2.0 for DSFGs. Different values of $\beta$ do not significantly affect our conclusion, yielding almost the same temperature and SPIRE colours. We included flux errors of ± 20 per cent in estimating the uncertainties in the SPIRE colours. Fig. 2 shows $S_{500}/S_{350}$ versus $S_{350}/S_{250}$ colour–colour diagram of the SPIRE sources in the three protoclusters.

We derived $L_{FIR}$ (8−1000 μm) by fitting single grey-body SEDs with $T_d$, a free parameter. From the sources selected based on the SPIRE colours, we further applied an FIR luminosity cut of $L_{FIR} \geq 5.0 \times 10^{12}$ $L_\odot$ for conservative searching for DSFGs. Thus, the lowest flux densities in our samples are (36.0, 30.0, 19.4) mJy for 2QZCluster, (28.8, 26.3, 15.2) mJy for HS1700, and (15.6, 19.2, 12.9) mJy for SSA22 in the SPIRE bands (250, 350, 500) μm, respectively. We finally obtained a sample of colour-selected bright SPIRE sources with colours consistent with the protocluster redshifts by rejecting ∼95 per cent of the 250 μm sources (thus we select just 12/643 (2 per cent), 26/579 (5 per cent), and 55/1253 (4 per cent) colour-selected bright SPIRE sources in 2QZCluster, HS1700, and SSA22). For COSMOS field, we applied the same colour selection as the three protoclusters to obtain a control sample of field galaxies. We have selected 111/4923 (2 per cent), 140/4923 (3 per cent), and 262/4923 (5 per cent) colour-selected bright SPIRE sources in COSMOS field for 2QZCluster, HS1700, and SSA22 (see also Table 2).

## 4 RESULTS

### 4.1 Search for overdensities

We searched for overdensities in an aperture with a radius of 6 comoving Mpc (3.8, 3.7, and 3.2 arcmin radius for $z = 2.2, 2.3$, and 3.1, respectively). This scale corresponds to physical scale of ∼1.5–2 Mpc radius for each protocluster redshift, matching the size of the overdensity of DSFGs around radio galaxies (e.g. Dannerbauer et al. 2014; Rigby et al. 2014). We put down a grid of these apertures every 10 arcsec for the protoclusters and COSMOS field,

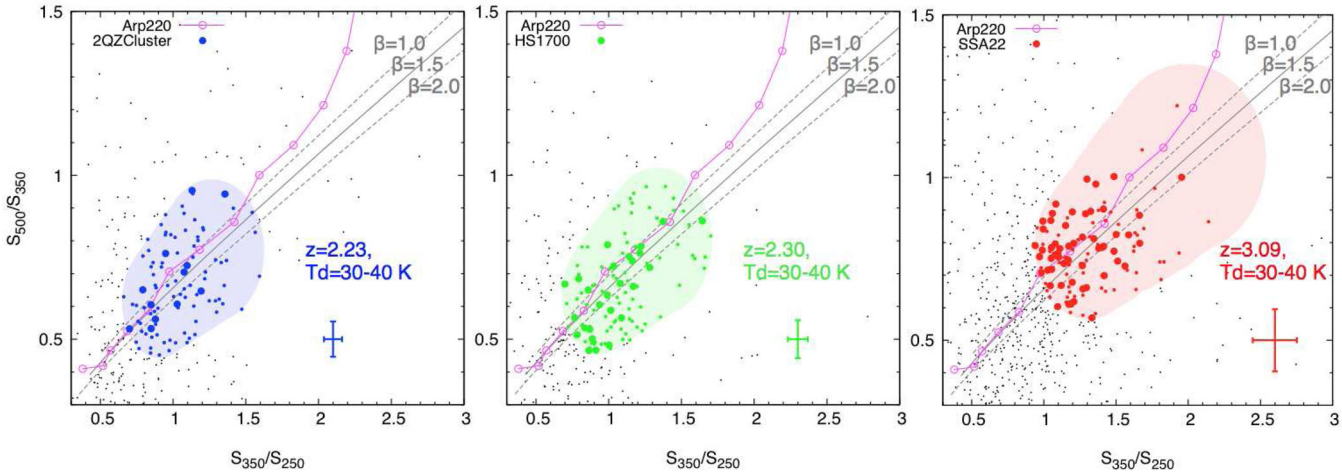


**Figure 2.** $S_{500}/S_{350}$ versus $S_{350}/S_{250}$ colour–colour diagram of the 250 μm sources. From left to right, we show the plots for 2QZCluster, HS1700, and SSA22. We selected candidates of DSFGs possibly associated with the protoclusters whose colours are consistent with a single grey-body SEDs including a photometric error of ± 20 per cent (shaded regions). We assume the protocluster redshifts, dust temperatures of $T_d$ = 30–40 K and dust emissivity $\beta = 1.5$. The grey solid and dashed lines show tracks of single grey-body SEDs for different $\beta$. We plot sources with fluxes above 12 mJy in least one SPIRE bands as small grey points. The coloured larger/smaller symbols show sources with $L_{FIR}$ larger/smaller than $5.0 \times 10^{12}$ $L_{\odot}$. The error bars show the average errors of colour-selected bright SPIRE sources. We have selected 2 per cent, 5 per cent, and 4 per cent colour-selected bright SPIRE sources to search for overdensities of DSFGs in 2QZCluster, HS1700, and SSA22. We plot the expected colours for Arp 220 as a function of redshifts (Polletta et al. 2007) for comparison. We plot open circles on track of Arp 220 every $z = 0.5$ from $z = 0$ to $z = 5.5$.

and counted the number of colour-selected bright SPIRE sources ($L_{FIR} \geq 5.0 \times 10^{12}$ $L_{\odot}$) within each aperture. For SSA22, we excluded a high background region (see in Fig. 3).

We found 3.9$\sigma$ and 5.0$\sigma$ overdensities in the 2QZCluster and HS1700 fields, respectively, but did not find any significant (>3$\sigma$) overdensities in the SSA22 field. We calculated the significance of overdensity, $\sigma_{pc} = (n_{pc} - n_{ave})/\sigma_{ave}$, where $n_{pc}$ is the number of colour-selected bright SPIRE sources in overdense region (6 comoving Mpc search radius) of the protocluster fields, $n_{ave}$ is the average number within a 6 comoving Mpc search radius for COSMOS field, and $\sigma_{ave}$ is the standard deviation of $n_{ave}$. We also searched for overdensities of colour-selected bright SPIRE sources in case for 10 per cent and 30 per cent flux error boundaries in Fig. 2. The result does not significantly change for 20 per cent and 30 per cent boundaries. We found that 30 per cent boundary shows same position of overdensities of colour-selected bright SPIRE sources compared with that of 20 per cent boundary in 2QZCluster and HS1700. We found 10 per cent boundary is not suitable because the number of colour-selected bright SPIRE sources are too small to search for overdensities. In Fig. 3, we show the sky distribution of the colour-selected bright SPIRE sources. We also show the density of 19 HAEs and 3 QSOs (Matsuda et al. 2011) for 2QZCluster, 45 LBGs for HS1700 (Rudie et al. 2012; Steidel et al. 2014), and 742 LAEs for SSA22 (Yamada et al. 2012), respectively.

We searched for overdensities of the colour-selected bright SPIRE sources in the COSMOS field in an identical manner as for the protocluster fields. We plot the density distribution of the colour-selected bright SPIRE sources for the 2QZCluster, HS1700, and COSMOS fields in Fig. 4. The histogram shows the distribution of the number of colour-selected bright SPIRE sources within a 6 comoving Mpc aperture (normalized by the number of searched apertures). We found that 2QZCluster has a low number of sources. The fraction of the apertures which have no sources is about two times higher compared with COSMOS field. This suggests that there is a void like distribution while there are also overdensities in 2QZCluster. In contrast, HS1700 tends to have larger number of colour-selected bright SPIRE sources in the search apertures.

We also plot the cumulative number of the circles in Fig. 4. We normalized the cumulative number of COSMOS field to the protoclusters. We found that the normalized cumulative number with >3.9$\sigma$ overdensities in 2QZCluster field is about two times higher than that in the COSMOS field. There are no overdensities in the COSMOS field which contain eight colour-selected bright SPIRE sources (5.0$\sigma$) as HS1700. This means that such overdensities are preferentially located in the protoclusters.

### 4.2 2QZCLUSTER

In the 2QZCluster field, an overdensity of colour-selected bright SPIRE sources were found 4.5 arcmin (∼2.2 Mpc) west to the HAEs overdensity.

We searched for the counterparts of SPIRE sources with HAEs and QSOs in 2QZCluster, which are summarized by Matsuda et al. (2011), although the SPIRE overdense region did not have H$\alpha$ image with United Kingdom Infrared Telescope (UKIRT)/Wide Field Camera (WFCAM) (see Fig. 3). In total, 19 HAEs and 3 QSOs are within the 174 arcmin$^2$ overlap region. We define the following quality criteria based on Downes et al. (1986) for assessing the robustness of identified candidate counterparts. We classify sources with $p \leq 0.05$ as secure counterparts, and those with $0.05 < p \leq 0.10$ as tentative counterparts. We calculated the $p$-value defined by $p = 1 - \exp(-\pi n \theta^2)$, where $n$ is the source density and $\theta$ is the angular offset. We searched for counterparts within 11 arcsec radius from the centre of the SPIRE sources. This search radius corresponds to ∼40 per cent beam response in 250 μm band.

For the QSOs, one optically luminous QSO, which is known as 2QZC-C1-HAE2 (Matsuda et al. 2011), coincides with one of our colour-selected bright SPIRE source 2QZCluster-SPIRE10 (2.7 arcsec offset). The $p$-value is lower than 0.01, suggesting a secure counterpart, the probability of chance association of counterparts is lower than 1 per cent. 2QZ-C1-HAE3 also coincides with our SPIRE source 2QZCluster-SPIRE124 (5.6 arcsec offset) as a secure counterpart. Such optically luminous FIR bright QSOs are thought to be in a transient phase between DSFGs and QSOs (Simpson et al.

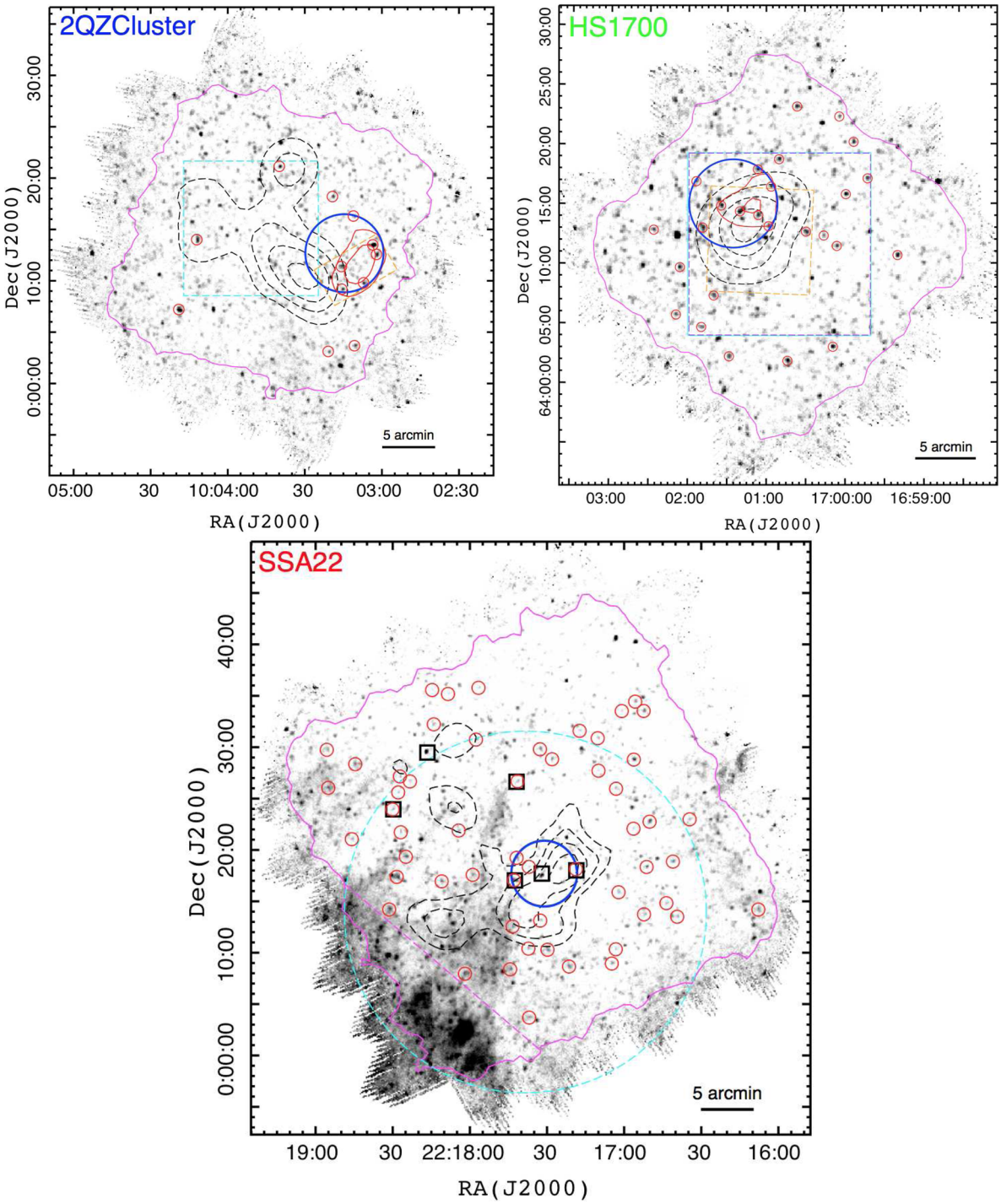


**Figure 3.** Sky distributions of colour-selected bright 250 μm sources (red circles) overplotted on the SPIRE 250 μm maps. The areas outlined with magenta contour corresponds to the 30 per cent depth coverage. For SSA22, we do not use below the dashed magenta line due to the high background fluxes. The dashed black contours show the density of 19 HAEs and 3 QSOs (Matsuda et al. 2011) for the 2QZCluster, 45 LBGs for HS1700 (Rudie et al. 2012; Steidel et al. 2014), and 742 LAEs for SSA22 (Yamada et al. 2012), respectively. The steps show $1\sigma$–$4\sigma$, $1\sigma$–$4\sigma$, and $3\sigma$–$6\sigma$ for 2QZCluster, HS1700, and SSA22 (smoothed with a Gaussian kernel with a FWHM of 6 comoving Mpc). The red contours show $3\sigma$–$4\sigma$, $4\sigma$–$5\sigma$ for colour-selected bright SPIRE sources in 2QZCluster and HS1700 with a same Gaussian kernel ($1\sigma$ is standard deviation of surface density of colour-selected bright SPIRE sources measured in COSMOS field). The large blue circles show the overdensity of colour-selected bright 250 μm sources for 2QZCluster and HS1700, and colour-selected bright 500 μm sources for SSA22 using filtering a radius of 6 comoving Mpc. We find a $4\sigma$ and $5\sigma$ overdensity in the 2QZCluster and HS1700 fields. We do not find any significant overdensities of 250 μm sources in SSA22, but we found six colour-selected bright 500 μm sources (black squares), and three sources are concentrated 3 arcmin (∼1.4 Mpc) east to the LAEs overdensity. The dashed cyan and orange boxes in 2QZCluster show the UKIRT/WFCAM (for HAEs) and Subaru/MOIRCS (for HAEs) coverage. The solid cyan, dashed purple, and orange boxes in HS1700 show the Keck/Low Resolution Imaging Spectrograph (LRIS) (for LAEs and LBGs, respectively) and Palomar/WIRC (for HAEs) coverage. The dashed cyan large circle in SSA22 shows Atacama Submillimeter Telescope Experiment (ASTE)/AzTEC coverage.

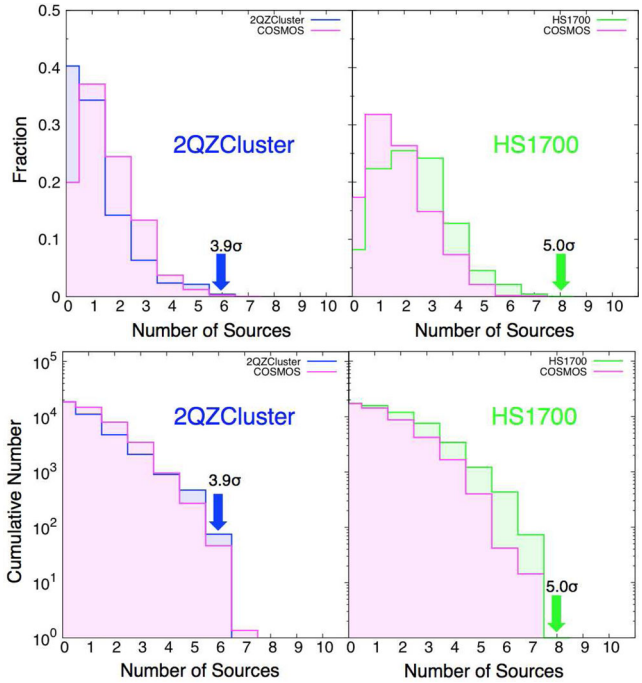


**Figure 4.** (Upper). The density distributions of the colour-selected bright SPIRE sources in 2QZCluster (left) and HS1700 (right) within an aperture radius of 6 comoving Mpc. 2QZCluster tends to have lower number of colour-selected bright SPIRE sources compared with COSMOS field. This could be explained if there are void-like structures within the survey area although there are also overdense regions. In contrast, HS1700 tends to have higher number of sources. (Lower). Cumulative number of the apertures with a radius of 6 comoving Mpc. We normalized the cumulative number of COSMOS field to the protoclusters.

2012). No other HAEs matched with colour-selected bright SPIRE sources. We then repeated this matching using all 250 μm sources, and found five secure HAE counterparts (see Table 10).

We recently conducted Subaru/Multi-Object InfraRed Camera and Spectrograph (MOIRCS) follow-up NB imaging observations in 2015 May 5 to search for new HAEs as well as counterparts of the SPIRE sources in the SPIRE overdense region (4 arcmin × 7 arcmin; dashed orange box in Fig. 3). The total exposure time of $K_s$ and NB data is each 1.5 and 2.4 ks, respectively. The 5$\sigma$ detection limit of NB < 19.8 (Vega) is almost the same as the previous HAE search depth (NB < 19.9 in Vega) by Matsuda et al. (2011).

We find no new HAE within the area. This may suggest that the area is actually a little underdense in terms of bright HAE, because Matsuda et al. (2011) claim an average field count of 0.09 per arcmin$^2$, which corresponds to two or three HAEs per MOIRCS field of view (FOV). Such void structures adjacent to protocluster has been reported previously (e.g. Koyama et al. 2013; Saito et al. 2015).

### 4.3 HS1700

In HS1700, the overdensity peak of colour-selected bright SPIRE sources coincides with that of the protocluster member galaxies (2.1 arcmin offset, corresponding to ∼1.0 Mpc).

We searched for the counterparts of SPIRE sources using UV-selected (BX/BM) star-forming galaxies (LBGs), HAEs, LAEs, and Distant Red Galaxies (DRGs) in the SPIRE overdense region. There are 3010 LBGs within 256 arcmin$^2$, 123 LAEs are within 219 arcmin$^2$, 83 HAEs and 75 DRGs are within 72 arcmin$^2$. The LBG catalogues are from the KBSS (Keck Baryonic Structure Survey; Rudie et al. 2012; Steidel et al. 2014). HS1700 is one of the 15 QSO fields intensively studied in KBSS. The H$\alpha$ and Ly$\alpha$ NB catalogues are from Milan Bogosavljević's PhD thesis (Bogosavljević 2010). Individual properties of LBGs, LAEs and observations are described in Shapley et al. (2005), Erb et al. (2011), Kulas et al. (2013), and Erb et al. (2014). In addition, for the H$\alpha$ narrow-band imaging, we used the Br $\gamma$ filter (Palomar Wide Field Infrared Camera (WIRC), centre wavelength 2.17 μm, FWHM = 297 Å). The narrow band selection criteria are NB <20.5 (Vega) and NB $-K_s \leq -0.75$. The DRGs have selected with $J - K > 2.3$ to a limit of $K_s = 21$ (Vega). We define the quality criteria, and classify sources with $p$-value described above. We deduced the number density of 45 LBGs which have spectroscopically confirmed redshift in the protocluster (i.e. in the overdensity of $z = 2.285$–$2.315$) separately from remaining 2965 LBGs outside of overdensity. We searched for counterparts within 11 arcsec radius from the centre of the SPIRE sources.

We found three colour-selected bright SPIRE sources that have secure counterparts (see Table 11). But one of the LAEs BNB1, the spectrum of this object is extremely odd and that makes difficult to identify the redshift. We identified it as a Lo-BAL QSO and it is more likely to have $z \sim 2.00$, so we do not treat as it is a protocluster member galaxy.

We also found that one LAE and LBG are secure, and one DRG and LAE are tentative counterparts of colour-selected faint (i.e.

**Table 10.** Matching results for the SPIRE sources which have HAEs counterparts in 2QZCluster.

| ID (SPIRE) | RA (J2000) | Dec. (J2000) | $S_{250}$ (mJy) | $S_{350}$ (mJy) | $S_{500}$ (mJy) | Counterpart | RA (J2000) | Dec. (J2000) | Sepa.[a] (arcsec) | $p$-value[b] | Member[c] |
|---|---|---|---|---|---|---|---|---|---|---|---|
| Colour-selected bright SPIRE sources | | | | | | | | | | | |
| 2QZCluster-SPIRE10 | 150.916 320 | 0.352 456 | 60.1 ± 2.1 | 64.7 ± 1.8 | 45.6 ± 2.0 | QZC-C1-HAE02(QSO) | 150.915 790 | 0.353 000 | 2.73 | <0.01 | Secure |
| At least one SPIRE band above 12 mJy sources | | | | | | | | | | | |
| 2QZCluster-SPIRE124 | 150.965 998 | 0.249 463 | 21.9 ± 2.2 | 14.2 ± 1.8 | 9.7 ± 2.2 | QZC-C1-HAE03(QSO) | 150.964 920 | 0.250 583 | 5.60 | <0.01 | Secure |
| 2QZCluster-SPIRE239 | 151.069 470 | 0.310 488 | 15.4 ± 2.2 | 4.1 ± 1.8 | 6.9 ± 2.3 | QZC-C1-HAE20 | 151.069 750 | 0.309 167 | 4.86 | <0.01 | Secure |
| 2QZCluster-SPIRE251 | 150.885 551 | 0.168 325 | 15.5 ± 2.2 | 6.8 ± 2.0 | 3.7 ± 2.3 | QZC-C1-HAE09 | 150.887 370 | 0.167 917 | 6.71 | <0.01 | Secure |
| 2QZCluster-SPIRE261 | 150.852 526 | 0.155 903 | 15.8 ± 2.3 | 13.8 ± 1.8 | 12.1 ± 2.2 | QZC-C1-HAE05 | 150.854 380 | 0.155 694 | 6.72 | <0.01 | Secure |
| 2QZCluster-SPIRE353 | 150.916 183 | 0.187 292 | 14.4 ± 2.7 | 12.1 ± 1.8 | 3.0 ± 2.1 | QZC-C1-HAE16 | 150.915 750 | 0.187 722 | 2.20 | <0.01 | Secure |
| 2QZCluster-SPIRE372 | 150.935 267 | 0.238 716 | 10.2 ± 2.2 | 16.2 ± 1.8 | 14.0 ± 2.1 | QZC-C1-HAE15 | 150.932 670 | 0.238 944 | 9.39 | 0.01 | Secure |

[a]Separation between SPIRE source and counterparts.
[b]$p$-value based on Downes et al. (1986).
[c]We classify sources with $p \leq 0.05$ as secure, and those with $0.05 < p \leq 0.10$ as tentative counterparts.

**Table 11.** Matching results for the SPIRE sources which have emitter counterparts within overdensity in HS1700.

| ID (SPIRE) | RA (J2000) | Dec. (J2000) | $S_{250}$ (mJy) | $S_{350}$ (mJy) | $S_{500}$ (mJy) | ID (Count.) | RA (J2000) | Dec. (J2000) | $z^a$ | Sepa.[b] (arcsec) | $p$-value[c] | Member[d] |
|---|---|---|---|---|---|---|---|---|---|---|---|---|
| | | | | | Colour-selected bright SPIRE sources | | | | | | | |
| HS1700-SPIRE21 | 255.3951 | 64.2484 | 52.5 ± 2.2 | 41.2 ± 1.7 | 21.1 ± 2.2 | BNB1 | 255.3953 | 64.2479 | ∼2.00[e] | 1.63 | <0.01 | Secure |
| | | | | | | BX980 | 255.3987 | 64.2490 | – | 6.13 | 0.32 | Not |
| HS1700-SPIRE42 | 255.2428 | 64.2196 | 40.0 ± 2.3 | 46.4 ± 1.8 | 34.3 ± 2.1 | DRG46 | 255.2419 | 64.2195 | – | 1.37 | <0.01 | Secure |
| | | | | | | HaNB2 | 255.2417 | 64.2196 | – | 1.75 | <0.01 | Secure |
| HS1700-SPIRE24 | 255.3349 | 64.2403 | 51.5 ± 2.3 | 63.0 ± 2.0 | 49.3 ± 2.2 | DRG53 | 255.3378 | 64.2395 | ∼2.3[f] | 5.36 | 0.03 | Secure |
| | | | | | | HaNB10* | 255.3399 | 64.2384 | 2.289(abs) | 10.43 | 0.10 | Tentative |
| | | | | | | BX913* | 255.3399 | 64.2385 | 2.289(abs), 2.291(neb) | 10.29 | 0.05 | Tentative |
| | | | | | | BX928 | 255.3318 | 64.2405 | 2.755(Ly $\alpha$) | 4.92 | 0.22 | Not |
| | | | | | Colour-selected faint SPIRE sources | | | | | | | |
| HS1700-SPIRE321 | 255.2732 | 64.2046 | 13.7 ± 2.4 | 20.2 ± 1.8 | 15.9 ± 2.1 | BNB41* | 255.2688 | 64.2027 | 2.287(abs) | 9.64 | 0.05 | Secure |
| | | | | | | MD109* | 255.2687 | 64.2026 | 2.293(abs,neb) | 10.09 | 0.02 | Secure |
| | | | | | | DRG38$^+$ | 255.2669 | 64.2032 | 2.286(emi) | 10.98 | 0.10 | Tentative |
| | | | | | | BNB16$^+$ | 255.2670 | 64.2033 | 2.290(emi) | 10.53 | 0.05 | Tentative |
| | | | | | At least one SPIRE band above 12 mJy sources | | | | | | | |
| HS1700-SPIRE70 | 255.2827 | 64.2586 | 31.1 ± 2.2 | 21.4 ± 1.9 | 11.0 ± 2.0 | BNB155 | 255.2811 | 64.2574 | 2.290(Ly $\alpha$) | 5.13 | 0.01 | Secure |
| | | | | | | HaNB27 | 255.2873 | 64.2578 | – | 7.81 | 0.06 | Tentative |
| HS1700-SPIRE78 | 255.4358 | 64.2607 | 30.3 ± 2.2 | 16.9 ± 1.7 | 6.0 ± 2.1 | BNB139 | 255.4331 | 64.2622 | – | 6.85 | 0.02 | Secure |
| HS1700-SPIRE142 | 255.2668 | 64.2469 | 22.7 ± 2.2 | 12.0 ± 1.8 | 1.8 ± 2.2 | HaNB83 | 255.2653 | 64.2487 | – | 6.67 | 0.04 | Secure |
| | | | | | | HaNB76 | 255.2661 | 64.2461 | – | 3.06 | 0.01 | Secure |
| HS1700-SPIRE179 | 255.3768 | 64.1988 | 19.8 ± 2.2 | 9.4 ± 1.8 | 0.5 ± 2.2 | HaNB45 | 255.3796 | 64.1996 | – | 5.41 | 0.03 | Secure |

[a]Redshift information of counterparts.
[b]Separation between SPIRE source and counterparts.
[c]$p$-value based on Downes et al. (1986).
[d]We classify sources with $p \leq 0.05$ as secure, and those with $0.05 < p \leq 0.10$ as tentative counterparts.
[e]BNB1 is identified as a "Lo-BAL" QSO and therefore it is difficult to measure redshift.
[f]Photometric redshift from Chapman et al. (2015).

$L_{\rm FIR} < 5.0 \times 10^{12}$ L$_\odot$) SPIRE source. For the SPIRE sources which are not selected with our colour selection, but have at least one SPIRE band above 12 mJy, we found two secure LAEs, three secure HAEs, and one tentative HAE. Thus, we conclude that seven SPIRE sources in the overdensity have secure counterparts of protocluster galaxies (see Table 11).

In order to assess the success rate of the SPIRE colour selection, we compared the matching result for colour-selected bright/faint SPIRE sources and all 250 μm sources lying within overdensity. We assumed that all HAEs and LAEs are associated with the protocluster except for BNB1, although we should note that the HAEs without spectroscopic follow-up are much less likely than spectroscopic confirmed HAEs to be at the cluster redshift. For all secure counterparts, the fractions are 2/7 (29 per cent), 1/5 (20 per cent), and 4/28 (14 per cent), respectively. This suggests that our SPIRE colour selection can select possible protocluster members with three times higher probability compared to not colour-selected sources.

In the HS1700 field, there are several foreground galaxy groups in the field. A $z = 0.453$ group is very close to the position of HS1700-SPIRE24. Indeed, Peter et al. (2007) found that BX913 is lensed by the group. We calculated a magnification factor by using GLAFIC (Oguri 2010). We used a halo mass of $M/h = 1 \times 10^{14}$ M$_\odot$ (Israel et al. 2014) and a concentration parameter of $c = 6$ (Bhattacharya et al. 2013). We found that the second nearest (1.5 arcmin away from group centre) SPIRE source is affected only ∼5 per cent magnification, so we conclude that only the HS1700-SPIRE24 could be affected by lensing.

### 4.4 SSA22

The maximum number of colour-selected bright SPIRE sources found in 6 comoving Mpc aperture was five, corresponding to a 1.6$\sigma$ overdensity. This suggests that SSA22 does not have any significant overdensities of colour-selected bright 250 μm sources. But, this could be a problem for SSA22 at $z = 3.1$ because DSFGs would start to drop out at 250 μm. Here, we searched for an overdensity of colour-selected bright 500 μm detected sources with identical colour selection and luminosity cut in Section 3.2. We found six colour-selected bright 500 μm sources in the SSA22 field, and three sources are concentrated 3 arcmin (∼1.4 Mpc) east to the LAEs overdensity (Fig. 3). For 350 μm sources, we did not find any significant overdensities as same as 250 μm sources.

We investigated AzTEC 1.1 mm counterparts in Umehata et al. (2014, 2015) for the five colour-selected bright 500 μm sources within ∼800 arcmin$^2$ overlapped region (Fig. 3). We searched for the counterparts within a radius of 14 arcsec (half of AzTEC 1.1 mm FWHM). We found that four colour-selected bright 500 μm sources have been matched (SSA22-AzTEC1, 2, 5, and 34). Thus ∼80 per cent colour-selected bright 500 μm sources are matched with AzTEC 1.1 mm sources.

## 5 DISCUSSION AND SUMMARY

We searched for DSFGs associated with three protoclusters at $z =$ 2–3 (2QZCluster, HS1700, SSA22) using *Herschel*/SPIRE. In the 2QZCluster and HS1700 field, we found 4$\sigma$ and 5$\sigma$ overdensities of the colour-selected bright SPIRE sources on a scale of 6 comoving Mpc. In the SSA22, we did not find any significant overdensities of 250 μm sources, but we found that three colour-selected bright 500 μm sources are concentrated on a scale of 6 comoving Mpc. The results suggest possible activity associated with enhanced dusty star formation in protoclusters at $z \sim 2$–3.

We derive the SFR density of 2QZCluster, HS1700, and SSA22 to compare with the average value of the Universe. The SFR of DSFGs is often converted from FIR luminosity, although the conversion from $L_{\rm FIR}$ to SFR is not straightforward and relies on the dust composition and initial mass function (IMF). Most works on DSFGs assume the conversion given by SFR (M$_\odot$ yr$^{-1}$) = $4.5 \times 10^{-44}$ $L_{\rm FIR}$ (erg s$^{-1}$) or $1.7 \times 10^{-10}$ $L_{\rm FIR}$ ($L_\odot$) (Kennicutt 1998), where $L_{\rm FIR}$ is the integrated luminosity of 8−1000 μm. This conversion takes the radiative transfer models of Leitherer & Heckman (1995) and a Salpeter IMF (Salpeter 1955).

We used a simple estimation to calculate the integrated SFR densities by assuming that all colour-selected bright SPIRE sources in the overdensities are associated with protoclusters. In addition, we also included sources with S/N > 2 in all three SPIRE bands within a radius of 1 Mpc (physical) following Clements et al. (2014) analysis of *Planck* clumps with *Herschel*/SPIRE. Because this radius of 1 Mpc circles is smaller than our search radius (6 comoving Mpc, ∼1.5–2 Mpc in physical), we adjusted the position of the smaller aperture to contain as many colour-selected bright SPIRE sources as possible. This enables us to select regions similar to *Planck* clumps in Clements et al. (2014). The 1$\sigma$ instrumental noise of Clements's work ranges from 2.5 to 2.8 mJy at 250 μm, 2.1 to 2.3 mJy at 350 μm, and 3.0 to 3.3 mJy at 500 μm (Clements et al. 2014), which is similar to our survey. For all SPIRE sources within a 1 Mpc radius, we fitted single grey-body SEDs with fixed $T_d =$ 35 K, $\beta = 1.5$ and the protocluster's redshifts, and derived $L_{\rm FIR}$. We excluded one colour-selected bright SPIRE source HS1700-SPIRE30 from this discussion because it is very close to $z = 0.08$ Sloan Digital Sky Survey (SDSS) galaxy, and its *Spitzer*/Multiband Imaging Photometer for Spitzer (MIPS) 24 μm flux density is very high (∼200 μJy). We found that MIPS 24 μm flux densities of other colour-selected bright SPIRE sources in HS1700 are consistent with that of typical high-$z$ star-forming galaxies. 2QZCluster does not have any *Spitzer* images.

Fig. 5 shows our results and compare to previous studies in the literature. We calculated SFR with Bell (2003)'s $L_{\rm FIR}$ correction to follow Clements et al. (2014) analysis. The derived SFR densities are $10^3$–$10^4$ times higher than the global SFR density seen in Madau & Dickinson (2014). This comparison indicates enhanced star formation activities in protoclusters at $z \sim 2$–3. The enhancement of dusty star-formation activity within our protoclusters is consistent with that seen for *Planck* clumps (Clements et al. 2014). Dannerbauer et al. (2014) presents results based on Atacama Pathfinder EXperiment telescope (APEX)/Large Apex BOlometer CAmera (LABOCA) 870 μm observations around MRC1138−262 at $z = 2.16$, showing that at least six DSFGs are likely part of the protocluster. The SFR density ∼1500 M$_\odot$ yr$^{-1}$ Mpc$^{-3}$ is similar to Clements et al. (2014) and our protoclusters study. We also plot the error bars in Fig. 5. The high end shows the case when including all sources in 1 Mpc radius and the low end shows the case for subtracting field average values. We deduced field values by calculating average number of sources and average luminosity in 1 Mpc radius apertures in the COSMOS field.

In Table 12, we summarized the estimated SFR and assumed volume plotted in Fig. 5. We also calculated SFR density in an aperture using a radius of 6 comoving Mpc in the same manner. These radii are 1.9, 1.8, and 1.5 Mpc in physical units for 2QZCluster, HS1700, and SSA22, respectively, and the results do not change compared to the case of 1 Mpc.

What causes the enhanced dusty star-forming activity in our protoclusters? One possible answer to this is galaxies mergers. For instance, Casey et al. (2015) investigated the morphology of the

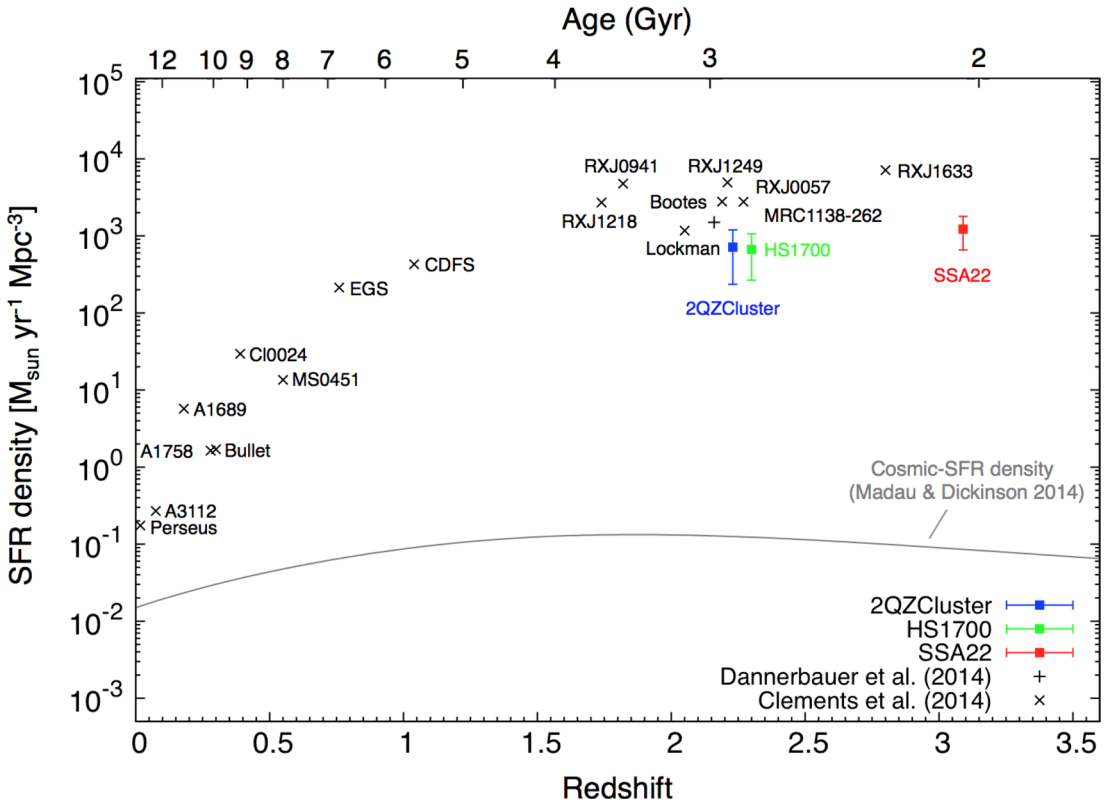


**Figure 5.** SFR density of clusters, protoclusters, and global cosmic SFR densities. The SFR densities of our protoclusters are $10^3$–$10^4$ times higher than the global SFR density (Madau & Dickinson 2014). We show the compilation from Dannerbauer et al. (2014) and data from Clements et al. (2014), which original literature are following; *IRAS* measurements of Perseus from Meusinger, Brunzendorf & Krieg (2000), Balloon-borne Large Aperture Submillimeter Telescope (BLAST) measurements of A3112 from Braglia et al. (2011), *ISO* measurements of A1689 from Fadda et al. (2000), and *Spitzer* measurements of A1758 from Haines et al. (2009), Bullet cluster from Chung et al. (2010), Cl0024+16 and MS0451-03 from Geach et al. (2006). RXJ0057, RXJ0941, RXJ1218, RXJ1249, and RXJ1633 are based on James Clerk Maxwell Telescope/Submillimetre Common-User Bolometer Array from Stevens et al. (2010).

**Table 12.** Estimated SFR and assumed volume for Fig. 5.

| Field | $z$ | SFR[a] ($M_\odot$ yr$^{-1}$) | $r$[b] (Mpc) | $V$[c] (Mpc$^3$) | SFR$_{min}$[d] ($M_\odot$ yr$^{-1}$) |
|---|---|---|---|---|---|
| | | All sources | | | |
| 2QZCluster | $2.230 \pm 0.016$ | 5000 | 1.0 | 4.2 | 150 |
| HS1700 | $2.300 \pm 0.015$ | 4500 | 1.0 | 4.2 | 280 |
| SSA22 | $3.09 \pm 0.03$ | 7500 | 1.0 | 4.2 | 310 |
| | | Field-corrected values | | | |
| 2QZCluster | $2.230 \pm 0.016$ | 1000 | 1.0 | 4.2 | – |
| HS1700 | $2.300 \pm 0.015$ | 2000 | 1.0 | 4.2 | – |
| SSA22 | $3.09 \pm 0.03$ | 4700 | 1.0 | 4.2 | – |

[a]Integrated SFR derived from SPIRE sources which are included in column 4 radius.
[b,c]Used radius and volume to calculate SFR density.
[d]Minimum SFR of SPIRE source which is included in integrated SFR.

galaxies in a protocluster to search for interaction/merger state by using *Hubble Space Telescope H*-band imaging data. Although the sample size is limited, they found that the fraction of irregular and interacting galaxies among the LBGs and DSFGs is 1.5 times higher in the protocluster than in the field. Webb et al. (2015) suggested that dusty star formation at the centre of a $z = 1.7$ cluster is being driven by galaxy–galaxy interaction, involving a FIR luminous bright cluster galaxy. Because there are strong correlation between the major-merger and the FIR luminosity (Engel et al. 2010; Kartaltepe et al. 2010, 2012; Hung et al. 2013), higher major mergers rate in protoclusters could induce dusty star formation. *N*-body simulation also predicts that progenitors of cluster and group haloes at $z > 2$ have 3–5 × higher major merger rates than isolated haloes (Gottlöber, Klypin & Kravtsov 2001). The fact that the colour-selected bright SPIRE sources are significantly concentrated in HS1700 and 2QZCluster would support such simultaneously major merging phenomenon. However, further observations are needed to investigate the processes of dusty star-forming activity in these protoclusters.

## ACKNOWLEDGEMENTS

We thank the anonymous referee for helpful comments which significantly improved the clarity of this paper. We thank Scott Chapman, James Colbert, Emanuele Daddi, Koichiro Nakanishi, and Kazuhiro Shimasaku for useful discussions and supports. Rhythm Shimakawa and Mariko Kubo made enormous contribution to analyses. We acknowledge Masaru Kajisawa for our use of his MOIRCS fringe-removal software (Kajisawa et al. 2015) during the data reduction.

*Herschel* is an ESA space observatory with science instruments provided by European-led Principal Investigator consortia and with important participation from NASA. SPIRE has been developed by a consortium of institutes led by Cardiff University (UK). Subaru Telescope, which is operated by the National Astronomical Observatory of Japan. UKIRT is funded by the STFC (UK). The W.M. Keck Observatory was made possible by the generous financial support of the W.M. Keck Foundation. The authors wish to recognize and acknowledge the very significant cultural role and

reverence that the summit of Mauna Kea has always had within the indigenous Hawaiian community. We are most fortunate to have the opportunity to conduct observations from this mountain.

This research was supported in part by a grant from the Hayakawa Satio Fund awarded by the Astronomical Society of Japan. YM acknowledges support from JSPS KAKENHI Grant Number 20647268. IRS acknowledges support from STFC (ST/L00075X/1), the ERC Advanced Grant DUSTYGAL (321334), and a Royal Society/Wolfson Merit Award. BH acknowledges support from JSPS KAKENHI Grant Number 15K17616. HU acknowledges support from Grant-in-Aid for JSPS Fellows, 26.11481.

## REFERENCES

Bell E. F., 2003, ApJ, 586, 794
Béthermin M. et al., 2012, A&A, 542, AA58
Bhattacharya S., Habib S., Heitmann K., Vikhlinin A., 2013, ApJ, 766, 32
Bogosavljević M., 2010, PhD thesis, California Inst. Technol.
Braglia F. G. et al., 2011, MNRAS, 412, 1187
Brodwin M. et al., 2013, ApJ, 779, 138
Casey C. M., 2016, ApJ, 824, 36
Casey C. M. et al., 2012, ApJ, 761, 140
Casey C. M. et al., 2015, ApJ, 808, L33
Chapman S. C. et al., 2015, MNRAS, 449, L68
Chung S. M., Gonzalez A. H., Clowe D., Markevitch M., Zaritsky D., 2010, ApJ, 725, 1536
Clements D. L. et al., 2014, MNRAS, 439, 1193
Croom S. M., Smith R. J., Boyle B. J., Shanks T., Loaring N. S., Miller L., Lewis I. J., 2001, MNRAS, 322, L29
Croom S. M., Smith R. J., Boyle B. J., Shanks T., Miller L., Outram P. J., Loaring N. S., 2004, MNRAS, 349, 1397
Dannerbauer H. et al., 2014, A&A, 570, AA55
Digby-North J. A. et al., 2010, MNRAS, 407, 846
Downes A. J. B., Peacock J. A., Savage A., Carrie D. R., 1986, MNRAS, 218, 31
Elbaz D. et al., 2007, A&A, 468, 33
Ellis R. S., Smail I., Dressler A., Couch W. J., Oemler A., Jr, Butcher H., Sharples R. M., 1997, ApJ, 483, 582
Engel H. et al., 2010, ApJ, 724, 233
Erb D. K., Bogosavljević M., Steidel C. C., 2011, ApJ, 740, L31
Erb D. K. et al., 2014, ApJ, 795, 33
Fadda D., Elbaz D., Duc P.-A., Flores H., Franceschini A., Cesarsky C. J., Moorwood A. F. M., 2000, A&A, 361, 827
Geach J. E. et al., 2006, ApJ, 649, 661
Gottlöber S., Klypin A., Kravtsov A. V., 2001, ApJ, 546, 223
Granato G. L., Ragone-Figueroa C., Domínguez-Tenreiro R., Obreja A., Borgani S., De Lucia G., Murante G., 2015, MNRAS, 450, 1320
Griffin M. J. et al., 2010, A&A, 518, L3
Haines C. P., Smith G. P., Egami E., Okabe N., Takada M., Ellis R. S., Moran S. M., Umetsu K., 2009, MNRAS, 396, 1297
Hayashino T. et al., 2004, AJ, 128, 2073
Hildebrand R. H., 1983, Q. J. R. Astron. Soc., 24, 267
Hung C.-L. et al., 2013, ApJ, 778, 129
Israel H., Reiprich T. H., Erben T., Massey R. J., Sarazin C. L., Schneider P., Vikhlinin A., 2014, A&A, 564, A129
Ivison R. J., Dunlop J. S., Smail I., Dey A., Liu M. C., Graham J. R., 2000, ApJ, 542, 27
Ivison R. J. et al., 2013, ApJ, 772, 137
Kajisawa M., Morishita T., Taniguchi Y., Kobayashi M. A. R., Ichikawa T., Fukui Y., 2015, ApJ, 801, 134
Kartaltepe J. S. et al., 2010, ApJ, 721, 98
Kartaltepe J. S. et al., 2012, ApJ, 757, 23
Kennicutt R. C., Jr, 1998, ARA&A, 36, 189
Koyama Y., Kodama T., Tadaki K.-i., Hayashi M., Tanaka M., Smail I., Tanaka I., Kurk J., 2013, MNRAS, 428, 1551
Kulas K. R. et al., 2013, ApJ, 774, 130
Lehmer B. D. et al., 2009a, MNRAS, 400, 299
Lehmer B. D. et al., 2009b, ApJ, 691, 687
Lehmer B. D. et al., 2013, ApJ, 765, 87
Leitherer C., Heckman T. M., 1995, ApJS, 96, 9
Lilly S. et al., 1998, ApJ, 500, 75
Lutz D. et al., 2001, A&A, 378, 70
Ma C.-J. et al., 2015, ApJ, 806, 257
Madau P., Dickinson M., 2014, ARA&A, 52, 415
Matsuda Y. et al., 2004, AJ, 128, 569
Matsuda Y. et al., 2011, MNRAS, 416, 2041
Meusinger H., Brunzendorf J., Krieg R., 2000, A&A, 363, 933
Nguyen H. T. et al., 2010, A&A, 518, L5
Oguri M., 2010, PASJ, 62, 1017
Oliver S. J. et al., 2012, MNRAS, 424, 1614
Peter A. H. G., Shapley A. E., Law D. R., Steidel C. C., Erb D. K., Reddy N. A., Pettini M., 2007, ApJ, 668, 23
Pilbratt G. L. et al., 2010, A&A, 518, L1
Polletta M. et al., 2007, ApJ, 663, 81
Rigby E. E. et al., 2014, MNRAS, 437, 1882
Rudie G. C. et al., 2012, ApJ, 750, 67
Saito T. et al., 2015, MNRAS, 447, 3069
Salpeter E. E., 1955, ApJ, 121, 161
Shapley A. E., Steidel C. C., Erb D. K., Reddy N. A., Adelberger K. L., Pettini M., Barmby P., Huang J., 2005, ApJ, 626, 698
Simpson J. M. et al., 2012, MNRAS, 426, 3201
Smail I., Ivison R. J., Blain A. W., Kneib J.-P., 1998, ApJ, 507, L21
Smail I. et al., 2014, ApJ, 782, 19
Smith A. J. et al., 2012, MNRAS, 419, 377
Steidel C. C., Adelberger K. L., Dickinson M., Giavalisco M., Pettini M., Kellogg M., 1998, ApJ, 492, 428
Steidel C. C., Adelberger K. L., Shapley A. E., Pettini M., Dickinson M., Giavalisco M., 2000, ApJ, 532, 170
Steidel C. C., Adelberger K. L., Shapley A. E., Erb D. K., Reddy N. A., Pettini M., 2005, ApJ, 626, 44
Steidel C. C. et al., 2014, ApJ, 795, 165
Stevens J. A. et al., 2003, Nature, 425, 264
Stevens J. A., Jarvis M. J., Coppin K. E. K., Page M. J., Greve T. R., Carrera F. J., Ivison R. J., 2010, MNRAS, 405, 2623
Swinyard B. M. et al., 2010, A&A, 518, L4
Tamura Y. et al., 2009, Nature, 459, 61
Tran K.-V. H. et al., 2010, ApJ, 719, L126
Umehata H. et al., 2014, MNRAS, 440, 3462
Umehata H. et al., 2015, ApJ, 815, L8
Valtchanov I. et al., 2013, MNRAS, 436, 2505
Webb T. et al., 2015, ApJ, 809, 173
Yamada T., Nakamura Y., Matsuda Y., Hayashino T., Yamauchi R., Morimoto N., Kousai K., Umemura M., 2012, AJ, 143, 79

## SUPPORTING INFORMATION

Additional Supporting Information may be found in the online version of this article:

**Table 3.** SPIRE sources catalogue of 2QZCluster.
**Table 4.** SPIRE sources catalogue of HS1700.
**Table 5.** SPIRE sources catalogue of SSA22.
(http://www.mnras.oxfordjournals.org/lookup/suppl/doi:10.1093/mnras/stw1237/-/DC1).

Please note: Oxford University Press is not responsible for the content or functionality of any supporting materials supplied by the authors. Any queries (other than missing material) should be directed to the corresponding author for the article.

This paper has been typeset from a TEX/LATEX file prepared by the author.